Equation of state and radii of finite nuclei in the presence of a diffuse surface layer

V. M. Kolomietz,[1] S. V. Lukyanov,[1] A. I. Sanzhur,[1] and S. Shlomo[2,3]
[1]*Institute for Nuclear Research, 03680 Kiev, Ukraine*
[2]*Cyclotron Institute, Texas A&M University, College Station, Texas 77843, USA*
[3]*Department of Elementary Particles and Astrophysics, the Weizmann Institute of Science, Rehovot 76100, Israel*
(Received 23 February 2017; published 8 May 2017)

The definitions of nuclear surface and nuclear radii are considered within the Gibbs-Tolman-Rowlinson-Widom (GTW) approach. We demonstrate the nonmonotonic behavior of the nuclear equimolar radii, which is due to the shell effects in the chemical potential of finite nuclei. The direct variational method within the extended Thomas-Fermi approximation is used to establish the equation of state for finite nuclei. We have studied the influence of the polarization effect caused by the neutron excess on the particle density and the nuclear radii. This effect increases with the asymmetry parameter X and can be responsible for the appearance of large neutron halos in nuclei well away from the β stability line. We have performed new calculations of the A dependence of the radii $R(A)$ of nucleon distribution, which are based on the use of the experimental data for the nuclear binding energy. We demonstrate the presence of the quantum shell effects in $R(A)$. We have analyzed the value of the neutron-skin thickness Δr_{np} in the isotopes of the Na, Sn, and Pb nuclei within the GTW approach and show the appearance of nonmonotonic behavior of Δr_{np} as a function of the neutron excess. We discuss the relative contributions to the neutron-skin thickness Δr_{np} from the skin and the halo effects.

DOI: 10.1103/PhysRevC.95.054305

I. INTRODUCTION

The nucleon distributions in finite nuclei possess surface diffuse layers which occur due to the quantum penetration of particles into the classically forbidden region. This fact creates the problem of the unambiguous definition of the nuclear surface and thereby of the nuclear size [1]. In particular, a strict definition of the nuclear surface and volume is needed to derive the surface tension σ, the incompressibility coefficient K, etc. Moreover, in a small finite system, such as a nucleus, the derivation of the equation of state (EOS) also meets some difficulties because of the uncertainty for the pressure in a system with a finite surface layer. In a classical liquid, the problem of the proper derivation of the surface of the finite drop in the presence of a diffuse interface was studied by Gibbs [2] Tolman [3], and Rowlinson and Widom (GTW) [4] where the concept of the equimolar dividing surface was used.

In the present paper we will apply the classical GTW approach to the nucleus as a quantum liquid drop focusing on the presence of the diffusive surface of the nucleon spatial distribution. The averaged characteristic of nucleon distribution is given by the root-mean-square (rms) radii for the neutron and proton, respectively. Evaluating the values of rms radii and the corresponding neutron-skin thicknesses, we adopt the extended Thomas-Fermi (ETF) and the direct variational methods [5,6]. The nucleon densities $\rho_p(r)$ and $\rho_n(r)$ are generated by the profile functions which are determined by the requirement that the energy of the nucleus should be stationary with respect to the variations of these profiles. The GTW concept is employed by introducing a dividing surface into the profile functions. We also study the problems of the nucleon redistribution within the surface region (nuclear periphery), in particular, the neutron coat and the neutron excess for nuclei far away from the β-stability line as well as the influence of the skin and halo effects on the value of the neutron-skin thickness.

This paper is an extension of our previous work [7] where the general equimolar GTW concept was adopted for nuclei with finite surface layers. In the present paper we apply the GTW approach to realistically determine the EOS for finite nuclei and some nuclear characteristics, such as the nuclear size, the surface tension, the pressure, etc. Taking into consideration the presence of a finite diffuse interface and applying the GTW approach, we redefine the surface and symmetry energies. The use of the GTW approach allows us to present a more realistic procedure for the extraction of the nuclear surface tension coefficient from the experimental data. In contrast to the previous work [7], we avoid the leptodermous approximation and improve the evaluation of the Coulomb energy taking into consideration the finite diffuse layer of the proton distribution. Following the GTW equimolar concept, we derive the curvature as well as the halo and skin effects on the surface energy and the surface component of symmetry energy.

This paper is organized as follows. In Sec. II we adopt the GTW model of an equimolar dividing surface for the two-component liquid drop with a finite surface layer. The application of the GTW model to some nuclear problems is considered in Secs. III–V. We conclude and summarize in Sec. VI.

II. EXTENSION OF THE GIBBS-TOLMAN-ROWLINSON-WIDOM CONCEPT FOR FINITE NUCLEI

Considering a nucleus which possesses the finite surface diffuse layer, we will follow the GTW concept of the equimolar dividing surface. We introduce the formal dividing surface of radius R, the corresponding volume $\mathcal{V} = 4\pi R^3/3$, and the surface area $\mathcal{S} = 4\pi R^2$. The dividing surface is arbitrary but located within the nuclear diffuse layer. The energy of a nucleus E as well as its mass number $A = N + Z$ and the

neutron excess $A_- = N - Z$ are split into the volume (bulk) and surface parts,

$$E = E_{\rm bulk} + E_{\mathcal{S}} + E_C, \quad A = A_{\mathcal{V}} + A_{\mathcal{S}},$$
$$A_- = A_{-,\mathcal{V}} + A_{-,\mathcal{S}}. \tag{1}$$

Here the Coulomb energy E_C is fixed and does not depend on the dividing radius R. The bulk energy $E_{\rm bulk}$ is identified with the energy E_∞ of the homogeneous nuclear matter,

$$E_{\rm bulk} = E_\infty, \tag{2}$$

and $E_{\mathcal{S}}$ is the surface energy [4,8],

$$E_{\mathcal{S}} = (\sigma + \mu\rho_{\mathcal{S}} + \mu_-\rho_{-,\mathcal{S}})\mathcal{S}, \tag{3}$$

with σ being the surface tension coefficient. The considered nuclear matter is the two-component one with isotopic asymmetry $X = (N - Z)/(N + Z)$ and chemical potentials,

$$\left.\frac{\partial E_{\rm bulk}}{\partial N}\right|_{\mathcal{V},Z} = \mu_n, \quad \left.\frac{\partial E_{\rm bulk}}{\partial N}\right|_{\mathcal{V},N} = \mu_p, \tag{4}$$

where n and p refer to a neutron and a proton, respectively.

The central assumption of the Gibbs-Tolman-Rowlinson-Widom approach is that the nuclear matter inside the specified volume $\mathcal{V}$ is chosen to have the chemical potentials μ_n and μ_p equal to the experimental values λ_n and λ_p of the corresponding nucleus, see also Ref. [9],

$$\mu_n(\rho_n, \rho_p) = \lambda_n - \lambda_{n,C}, \quad \mu_p(\rho_n, \rho_p) = \lambda_p - \lambda_{p,C}, \tag{5}$$

where ρ_n and ρ_p are the r-independent bulk densities of the neutrons and protons, respectively. The Coulomb contribution $\lambda_{q,C}$ to the nucleon chemical potential λ_q is subtracted in Eq. (5) because the derivation of μ_q in Eq. (4) is written for an uncharged nuclear matter. Here,

$$\lambda_{n,C} = \left.\frac{\partial E_C}{\partial N}\right|_Z, \quad \lambda_{p,C} = \left.\frac{\partial E_C}{\partial Z}\right|_N. \tag{6}$$

We also will use the isoscalar $\mu = (\mu_n + \mu_p)/2$, the isovector $\mu_- = (\mu_n - \mu_p)/2$, chemical potentials, and the corresponding densities $\rho = \rho_n + \rho_p$ and $\rho_- = \rho_n - \rho_p$. In agreement with the definition of the dividing surface adopted above, both densities ρ and ρ_- include the volume and surface parts,

$$\rho_{\mathcal{V}} = A_{\mathcal{V}}/\mathcal{V}, \quad \rho_{-,\mathcal{V}} = A_{-,\mathcal{V}}/\mathcal{V} \quad \text{and} \quad \rho_{\mathcal{S}} = A_{\mathcal{S}}/\mathcal{S},$$
$$\rho_{-,\mathcal{S}} = A_{-,\mathcal{S}}/\mathcal{S}. \tag{7}$$

The bulk energy $E_{\rm bulk}$ in Eqs. (2) and (4) can be evaluated using the Skyrme effective nucleon-nucleon interaction for the nuclear matter,

$$E_{\rm bulk} = \int d\boldsymbol{r}\ \epsilon_{\rm tot}(\boldsymbol{r}) \equiv \int d\boldsymbol{r}\ \epsilon_{\rm tot}[\rho_n(\boldsymbol{r}), \rho_p(\boldsymbol{r})]. \tag{8}$$

The total energy density functional of a nuclear matter $\epsilon_{\rm tot}[\rho_n, \rho_p]$ in Eq. (8) includes the kinetic-energy density $\epsilon_{\rm kin}[\rho_n, \rho_p]$ and the potential-energy density associated with the Skyrme interaction $\epsilon_{\rm Sk}[\rho_n, \rho_p]$,

$$\epsilon_{\rm tot}[\rho_n, \rho_p] = \epsilon_{\rm kin}[\rho_n, \rho_p] + \epsilon_{\rm Sk}[\rho_n, \rho_p]. \tag{9}$$

Considering an asymmetric nuclear matter with $X \ll 1$, the bulk energy per particle can be written as [5]

$$E_{\rm bulk}/A \equiv e_0(\rho) + e_2(\rho)\left(\frac{\rho_-}{\rho}\right)^2, \tag{10}$$

where

$$e_0 = \frac{\hbar^2}{2m}\alpha\rho^{2/3} + \frac{3t_0}{8}\rho + \frac{t_3}{16}\rho^{\nu+1} + \frac{\alpha}{16}[3t_1 + t_2(5 + 4x_2)]\rho^{5/3}, \tag{11}$$

and

$$e_2 = \frac{5}{9}\frac{\hbar^2}{2m}\alpha\rho^{2/3} - \frac{t_0}{8}(1 + 2x_0)\rho - \frac{t_3}{48}(1 + 2x_3)\rho^{\nu+1} + \frac{5\alpha}{72}[t_2(4 + 5x_2) - 3t_1x_1]\rho^{5/3}. \tag{12}$$

Here $\alpha = (3/5)(3\pi^2/2)^{2/3}$ and t_i, x_i, and ν are the Skyrme force parameters. The isoscalar and isovector chemical potentials are obtained from

$$\left.\frac{\partial E_{\rm bulk}}{\partial A}\right|_{\mathcal{V},A_-} = \mu, \quad \left.\frac{\partial E_{\rm bulk}}{\partial A_-}\right|_{\mathcal{V},A} = \mu_-. \tag{13}$$

The bulk equations (10)–(12) allow us to derive the equimolar radii of the nuclei. Using the experimental data for the separation energy s_q for each kind of nucleon, we obtain the corresponding chemical potentials $\lambda_n = -s_n$ and $\lambda_p = -s_p$. Applying then Eqs. (5), (10), and (13), we evaluate the bulk densities $\rho_{\mathcal{V}}$ and $\rho_{-,\mathcal{V}}$ and the surface densities $\rho_{\mathcal{S}}[R]$ and $\rho_{-,\mathcal{S}}[R]$. Note that the square brackets in $\rho_{\mathcal{S}}[R]$ and $\rho_{-,\mathcal{S}}[R]$ denote a formal dependence on the dividing radius R, which is arbitrary and may not correspond to the actual physical size of a nucleus. To derive the actual (equimolar) radius R_e of a nucleus, an additional condition on the location of the dividing surface should be imposed. In general, the surface energy $E_{\mathcal{S}}[R]$ for an arbitrary dividing surface includes the contributions from the surface tension σ and from the binding energy of the particles within the surface layer [see the term $\sim(\rho_{\mathcal{S}}\mu + \rho_{-,\mathcal{S}}\mu_-)$ in Eq. (3)]. In agreement with the Gibbs-Tolman-Rowlinson-Widom concept, the actual equimolar radius R_e of the droplet is determined by the requirement that the contribution to $E_{\mathcal{S}}[R]$ from the bulk term in Eq. (3) should be excluded from the surface energy $E_{\mathcal{S}}[R]$. The last requirement can be satisfied if the following condition is fulfilled:

$$(\rho_{\mathcal{S}}\mu + \rho_{-,\mathcal{S}}\mu_-)_{R=R_e} = 0, \tag{14}$$

where μ and μ_- are taken under the condition of Eq. (5). Equation (14) represents the derivation of the equimolar radius R_e for an asymmetric nucleus with $N \neq Z$.

In the case of finite nuclei, we will adopt the extended Thomas-Fermi approximation for the kinetic-energy density [10],

$$\epsilon_{{\rm kin},q}[\rho_q] = \frac{\hbar^2}{2m}\left[\frac{3}{5}(3\pi^2)^{2/3}\rho_q^{5/3} + \beta\frac{(\nabla\rho_q)^2}{\rho_q} + \frac{1}{3}\nabla^2\rho_q\right], \tag{15}$$

and the effective Skyrme interaction for the potential energy. The total energy of the charged nucleus is given by

$$E_{\rm tot}\{\rho_q,\nabla\rho_q\} = E_{\rm kin}\{\rho_q,\nabla\rho_q\} + E_{\rm Sk}\{\rho_q,\nabla\rho_q\} + E_C\{\rho_p\}, \tag{16}$$

where $E_{\rm Sk}\{\rho_q,\nabla\rho_q\}$ is the potential energy of the Skyrme interaction, which includes the gradient dependent terms $\sim\nabla\rho_q$,

$$E_{\rm Sk}\{\rho_q,\nabla\rho_q\} = \int d\boldsymbol{r}\ \epsilon_{\rm Sk}[\rho_q,\nabla\rho_q]. \tag{17}$$

$\epsilon_{\rm Sk}[\rho_q,\nabla\rho_q]$ is the density of the potential energy of the Skyrme interaction, and $E_C\{\rho_p\}$ is the Coulomb energy. In our consideration, the potential-energy $E_{\rm Sk}\{\rho_q,\nabla\rho_q\}$ also includes the energy due to the spin-orbit interaction.

Following the direct variational method, we choose a trial function for $\rho_q(\boldsymbol{r})$ as a power of the Fermi function for $\rho_q(\boldsymbol{r})$ given by, see also Ref. [6],

$$\rho_q(\boldsymbol{r}) = \rho_{0,q}\left[1+\exp\left(\frac{r-R_q}{a_q}\right)\right]^{-\eta_q}, \tag{18}$$

where $\rho_{0,q}$, R_q, a_q, and η_q are the unknown variational parameters. Considering the asymmetric nuclei with $X = (N-Z)/A \ll 1$, we will introduce the isotopic particle densities, namely, the total density $\rho_{0,+} = \rho_{0,n} + \rho_{0,p}$ and the neutron excess density $\rho_{0,-} = \rho_{0,n} - \rho_{0,p}$ with $\rho_{0,-} \ll \rho_{0,+}$.

The profile functions $\rho_+(r)$ and $\rho_-(r)$ have to obey the condition that the numbers of neutrons and protons are conserved. For the ground state of the nucleus, the unknown parameters $\rho_{0,\pm}$, R_q, a_q, and η_q and the total energy $E_{\rm tot}$ itself can be obtained from the variational principle,

$$\delta(E-\lambda_n N-\lambda_p Z) = 0, \tag{19}$$

where the variation with respect to all possible small changes in $\rho_{0,\pm}$, R_q, a_q, and η_q is assumed. The Lagrange multipliers λ_n and λ_p are the chemical potentials of the neutrons and the protons, respectively, and both of them are fixed by the condition that the number of particles is conserved.

III. EQUATION OF STATE OF FINITE NUCLEI AND THE POLARIZATION EFFECT

The introduction of a sharp (nondiffuse) equimolar surface obviates the ambiguities in the derivation of the pressure, the incompressibility, and the equation of state for finite systems with finite diffuse layers of the surfaces. In particular, using the concept of equimolar radius R_e, the total energy (1) of a finite nucleus can be written in the following form of the Weizsäcker mass formula:

$$\begin{aligned} &E_{\rm tot}(\rho_0,A,X)/A \\ &\quad = e_0(\rho_0) + b_S(\rho_0)A^{-1/3} + [b_{V,\rm sym}(\rho_0) \\ &\qquad + b_{S,\rm sym}(\rho_0)\,A^{-1/3}]X^2 + E_C(\rho_0,A,X)/A, \end{aligned} \tag{20}$$

where $e_0(\rho_0)$ is the bulk energy of a symmetric nuclear matter, $b_S(\rho_0)$ is the surface energy coefficient, $b_{V,\rm sym}(\rho_0)$ is the volume part of the symmetry energy, $b_{S,\rm sym}(\rho_0)$ is its surface part, and

$$\rho_0(R_e) = A\,(3/4\pi)R_e^{-3}. \tag{21}$$

The Coulomb energy $E_C(\rho_0,A,X)$ can be written as

$$\begin{aligned} E_C(\rho_0,A,X) &= \alpha_C(\rho_0)(1-X)^2A^{5/3} + O(A^{4/3}), \\ \alpha_C(\rho_0) &= \frac{3}{20}e^2\left(\frac{4\pi\rho_0}{3}\right)^{\frac{1}{3}}. \end{aligned} \tag{22}$$

The structure of the total energy given by Eq. (20) is similar to the semiempirical mass formula which describes the average changes in the nuclear binding energy with the mass number. However, in contrast to the mass formula, the bulk density ρ_0 and the asymmetry parameter X are not necessarily at equilibrium. The asymmetry term $\sim X^2$ includes both the volume $b_{V,\rm sym}(\rho_0)$ and the surface $b_{S,\rm sym}(\rho_0)$ contributions. The surface symmetry term $b_{S,\rm sym}(\rho_0)\ A^{-1/3}X^2$ appears in the advanced mass formula by Myers and Swiatecki [11,12], and it currently is employed in the description of surface properties and isovector excitations in finite nuclei, see, e.g., Refs. [13,14].

Similar to a classical liquid, the particle density ρ_0 in Eq. (20) is r independent, and the evaluation of the pressure $P(\rho_0)$ and thereby the equation of state can be obtained as in the classical case [8]. In the two-component nuclei, the form of the EOS is different for the isobaric case (fixed A and different X's) and the isotopic case (fixed Z and different X's). In the isobaric case, the EOS is derived as

$$\begin{aligned} P_A(\rho_0,X) &= -\left.\frac{\partial E_{\rm tot}(\rho_0,A,X)}{\partial V}\right|_{A,X} \\ &= \rho_0^2\left.\frac{\partial E_{\rm tot}(\rho_0,A,X)/A}{\partial\rho_0}\right|_{A,X}, \end{aligned} \tag{23}$$

where $E_{\rm tot}(\rho_0,A,X)$ is given by Eq. (20) with fixed A. In the isotopic case, the EOS is given by

$$\begin{aligned} P_Z(\rho_0,X) &= -\left.\frac{\partial E_{\rm tot}(\rho_0,Z,X)}{\partial V}\right|_{Z,X} \\ &= \rho_0^2\left.\frac{\partial E_{\rm tot}(\rho_0,Z,X)/A}{\partial\rho_0}\right|_{Z,X}, \end{aligned} \tag{24}$$

where $E_{\rm tot}(\rho_0,Z,X)$ is given by Eq. (20) with $A = 2Z(1-X)^{-1}$ and fixed Z.

For a given bulk density ρ_0, one can derive the isobaric β-stability line $X = X^*(A,\rho_0)$ by the condition,

$$\left.\frac{\partial E_{\rm tot}(\rho_0,A,X)}{\partial X}\right|_{A,\ X=X^*} = 0. \tag{25}$$

Near the β-stability line, the total energy (20) is written up to the order $(X-X^*)^2$ as

$$\begin{aligned} &E_{\rm tot}(\rho_0,A,X) \\ &\quad = E_{\rm tot}(\rho_0,A,X^*) + [b_{V,\rm sym}(\rho_0)A + b_{S,\rm sym}(\rho_0)A^{2/3} \\ &\qquad -\alpha_C(\rho_0)A^{5/3}](X-X^*)^2. \end{aligned} \tag{26}$$

The isotopic β-stability line $X = X^*(Z,\rho_0)$ is obtained from

$$\left.\frac{\partial E_{\rm tot}(\rho_0,Z,X)}{\partial X}\right|_{Z,\ X=X^*} = 0. \tag{27}$$

The derivation of nonequilibrium $\rho_0(R_e)$, Eqs. (20) and (21), and the corresponding EOS require model assumptions.

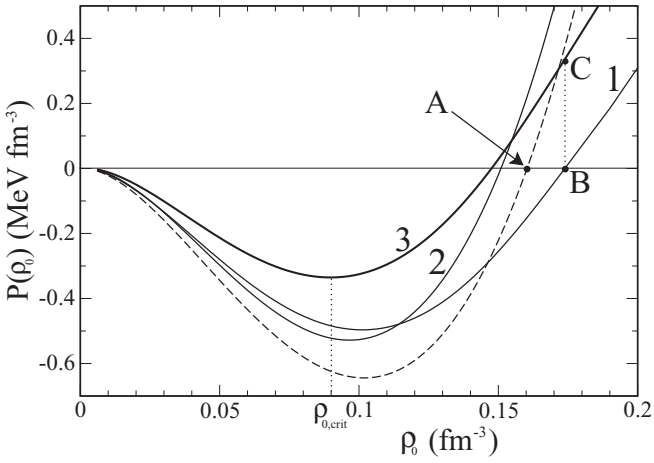

FIG. 1. Equation of state for the nucleus of ^{208}Pb. The calculation was performed for the SkM* interaction [15]. The dashed line is the EOS for the symmetric nuclear matter $P_{\rm vol}(\rho_0)$, solid line 1 is for $P_{\rm vol}(\rho_0)+P_{\rm capil}(\rho_0,X)$, solid line 2 is for $P_{\rm vol}(\rho_0)+P_C(\rho_0,X)$, and solid line 3 is the total pressure $P_A(\rho_0,X)$ of Eq. (28).

One of the appropriate models is the semiclassical ETF approximation which allows us to evaluate the nucleon density distribution $\rho_q(\boldsymbol{r})$ with a finite diffuse layer and the corresponding chemical potential λ_q [5]. The calculation of the bulk density ρ_0 and the equimolar radius R_e can then be performed by using the procedure described in Sec. II. In Fig. 1 we show the isobaric equation of state $P_A(\rho_0,X)$ for the nucleus of ^{208}Pb. Note that, in agreement with the general definition of Eq. (20), the pressure $P_A(\rho_0,X)$ includes: (i) the A- and X-independent bulk pressure $P_{\rm vol}(\rho_0)$ caused by the bulk energy of a symmetric nuclear matter $e_0(\rho_0)$, (ii) the surface (capillary) pressure $P_{A,\rm capil}(\rho_0,X)\sim A^{-1/3}$, (iii) the contribution from the symmetry energy $P_{A,\rm sym}(\rho_0,X)\sim X^2$, and (iv) the Coulomb force contribution $P_{A,C}(\rho_0,X)$,

$$P_A(\rho_0,X)=P_{\rm vol}(\rho_0)+P_{A,\rm capil}(\rho_0,X)+P_{A,\rm sym}(\rho_0,X)+P_{A,C}(\rho_0,X). \tag{28}$$

In agreement with Eq. (23) and the equilibrium condition,

$$\left.\frac{\partial E_{\rm tot}(\rho_0,A,X)}{\partial\rho_0}\right|_{\rho_0=\rho_{0,\rm eq}}=0, \tag{29}$$

the ground state of the nucleus is achieved at $P_A(\rho_0=\rho_{0,\rm eq},X)=0$. Using the SkM* [15] nucleon-nucleon interaction, we present the results for the EOS for the nucleus of ^{208}Pb in Fig. 1. As seen from Fig. 1, the inclusions of the surface (capillary) term $P_{\rm capil}(\rho_0,X)$ shift the equilibrium point to a larger value of $\rho_{0,\rm eq}$ (point B in Fig. 1) with respect to the one in a nuclear matter (point A in Fig. 1). Note that the capillary pressure $P_{A,\rm capil}(\rho_0,X)$ is connected to the surface tension coefficient $\sigma(A,X)$ by the Laplace relation [16],

$$P_{A,\rm capil}(\rho_0,X)=\frac{2\sigma(A,X)}{R_s}, \tag{30}$$

where R_s is the radius of tension (Laplace radius). The value of $P_{A,\rm capil}(\rho_0,X)$ is manifested by the straight dotted line BC in Fig. 1. The action of the Coulomb pressure $P_{A,C}(\rho_0,X)$ is opposite to the capillary pressure $P_{A,\rm capil}(\rho_0,X)$ and shifts the equilibrium point to the smaller values of $\rho_{0,\rm eq}$.

The radius R_s is shifted with respect to the equimolar radius R_e by a small value of $\xi=R_e-R_s$ (Tolman length [3]), which is caused by the finite diffuse layer in a nucleus [4,7,9]. Note also that the Tolman length ξ regulates the approach of the surface tension coefficient $\sigma(A,X)$ to the planar limit σ_∞ [4,17] in a semi-infinite system,

$$\sigma(R_e)=\sigma_\infty\left(1-\frac{2\xi}{R_e}+O\left(R_e^{-2}\right)\right). \tag{31}$$

The use of the Gibbs-Tolman equimolar radius R_e allows us to provide a more realistic procedure for the extraction of the nuclear surface tension coefficient from the experimental data. Note that the equimolar radius R_e determines the equimolar surface area $S_e=4\pi R_e^2$ in the absence of a diffuse layer. This fact gives the possibility to evaluate both the surface energy E_{S_e} and the surface tension coefficient $\sigma(A,X)=E_{S_e}/S_e$. The surface energy E_{S_e} is obtained by use of the experimental value of nuclear binding energy $E_{\rm exp}$ and the earlier derived bulk energy $E_{\rm bulk}$ of nuclear matter, see Eq. (10). Namely,

$$E_{S_e}=E_{\rm exp}-E_C-E_{\rm bulk}. \tag{32}$$

The Coulomb energy E_C is subtracted from the value of binding energy $E_{\rm exp}$ because the derivation of the nuclear matter energy $E_{\rm bulk}$ does not include the Coulomb energy contribution. Using the experimental data within the wide interval of mass number $40\leqslant A\leqslant 220$ and the corresponding values of equimolar radii, one can establish the following A expansion for the surface tension coefficient,

$$\begin{aligned}\sigma(A,X^*)&=\frac{E_{S_e}}{S_e}=\sigma_0+\frac{\sigma_1}{A^{1/3}},\\ \sigma_0&=(0.98\pm0.03)\ \text{MeV fm}^{-2},\\ \sigma_1&=(0.75\pm0.16)\ \text{MeV fm}^{-2}.\end{aligned} \tag{33}$$

The numerical result of Eq. (33) leads to the following value for the Tolman length ξ in nuclei:

$$\xi=(-0.41\pm0.07)\ \text{fm}. \tag{34}$$

Note that both values of σ_0 and σ_1 can also be derived from the capillary pressure $P_{A,\rm capil}(\rho_0,X)$ in Fig. 1. The corresponding values of σ_0 and σ_1 are close to those given in Eq. (33).

In Fig. 1, the minimum of the pressure $P_A(\rho_0,X)$ is located at $\rho_0=\rho_{0,\rm crit}$. The nucleus becomes unstable within the spinodal instability region $\rho_0<\rho_{0,\rm crit}$ where the incompressibility coefficient,

$$K_A(A,X)=9\left.\frac{\partial P_A(\rho_0,X)}{\partial\rho_0}\right|_{A,X}=9\,\rho_0^2\left.\frac{\partial^2 E_{\rm tot}(\rho_0,X)/A}{\partial\rho_0^2}\right|_{A,X} \tag{35}$$

is negative $K_A(A,X)<0$. In accordance with Eqs. (28) and (35), the incompressibility coefficient $K_A(A,X)$ includes the volume (nuclear matter) contribution K_{NM}, the surface term $K_{\rm surf}(A,X)$, the term $K_{\rm sym}(A,X)$ due to the symmetry energy,

and the Coulomb force contribution term $K_C(A,X)$. Namely,

$$K_A(A,X) = K_{NM} + K_{\rm surf}(A,X) + K_{\rm sym}(A,X) + K_C(A,X). \tag{36}$$

The equimolar radius R_e is A dependent. In general, the variation of the equimolar radius R_e with the nucleon number A is caused by two factors. There is the simple variation term of $R_e \propto A^{1/3}$ (see Fig. 5) and an additional term which occurs due to the polarization effect in nuclei away from the β-stability line because of the neutron excess $N-Z$. Considering the polarization effect, we will expand the total energy of Eq. (20) $E_{\rm tot}(\rho_0,A,X)/A$ around the equilibrium bulk density $\rho_{0,\rm eq}$. By keeping only terms quadratic in $\delta\rho_0 = \rho_0 - \rho_{0,\rm eq}$ we rewrite Eq. (20) as

$$\begin{aligned} &E_{\rm tot}(\rho_0,A,X)/A \\ &= E_{\rm tot}(\rho_{0,\rm eq},A,X^*)/A + \frac{K_A(A,X^*)}{18\rho_{0,\rm eq}^2}(\rho_0-\rho_{0,\rm eq})^2 \\ &+ \frac{P_{A,\rm sym}(\rho_{0,\rm eq},X^*)}{\rho_{0,\rm eq}^2}(X-X^*)^2(\rho_0-\rho_{0,\rm eq}), \end{aligned} \tag{37}$$

where

$$\begin{aligned} P_{A,\rm sym}(\rho_0) = \rho_0^2\frac{\partial}{\partial\rho_0}[&b_{V,\rm sym}(\rho_0) + b_{S,\rm sym}(\rho_0)\,A^{-1/3} \\ &- \alpha_C(\rho_0)A^{2/3}]. \end{aligned} \tag{38}$$

For an arbitrary fixed value of X, the equilibrium density $\rho_{0,X}$ is derived by the condition,

$$\frac{\partial}{\partial\rho_0}E_{\rm tot}(\rho_0,A,X)/A\Big|_{A,\rho_0=\rho_{0,X}} = 0. \tag{39}$$

Using Eqs. (37) and (39), one obtains the polarization effect on the particle density beyond the β-stability line,

$$\rho_{0,X} = \rho_{0,\rm eq}(X^*) - 9\frac{P_{A,\rm sym}(\rho_{0,\rm eq},X^*)}{K_A(A,X^*)}(X-X^*)^2. \tag{40}$$

In Fig. 2 we have plotted the partial pressure $P_{A,\rm sym}(\rho_0,X^*)$ versus the bulk density ρ_0 (partial equation of state) for the nucleus of ^{208}Pb, obtained using the SkM* [15], Sly230b [18], and KDE0v1 [19] Skyrme interactions. The dashed vertical line shows the position $\rho_0/\rho_{0,\rm crit} \approx 0.6$ of the spinodal instability border. On the left side of this line the nucleus is unstable with respect to the bulk density variations.

As seen from Fig. 2, the equilibrium value of the partial pressure $P_{A,\rm sym}(\rho_{0,\rm eq})$ is positive and thereby $\rho_{0,X} < \rho_{0,\rm eq}$, see also Refs. [20,21]. The partial pressure $P_{A,\rm sym}$ is rather sensitive to the Skyrme interaction parametrization (see results for the SkM*, SLy230b, and KDE0v1 in Fig. 2). The polarization effect also influences the equimolar radius R_e. The final result reads

$$R_e(A,X) = R_e^*(A,X^*)\left(1+\frac{1}{3}\frac{P_{A,\rm sym}(\rho_{0,\rm eq},X^*)}{K_A(A,X^*)\rho_{0,\rm eq}}(X-X^*)^2\right). \tag{41}$$

The magnitude of the polarization effect on the equimolar radius R_e can also be seen in Fig. 3 where we compare the A dependence of the equimolar radius $R_e = R_e^*(A,X^*)$ for the nuclei on the β-stability line in the presence of the partial polarization pressure $P_{A,\rm sym}(\rho_{0,\rm eq},X^*)$ (solid line) and with the $R_e(A,X=0)$ where the polarization pressure is ignored (dashed line).

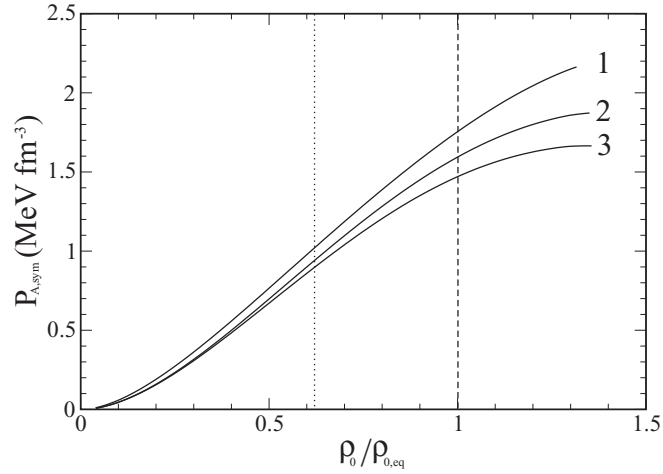

FIG. 2. The partial pressure $P_{A,\rm sym}$ for the nucleus of ^{208}Pb calculated for different parametrizations of the Skyrme forces: KDE0v1 [19]: solid line 1; SLy230b [18]: solid line 2; and SkM* [15]: solid line 3. The dotted vertical line is the mark for the spinodal instability border, and the dashed line is for the equilibrium density.

Considering the symmetric nuclei with $X=0$, one can estimate the polarization effect due only to the Coulomb interaction. Using Eq. (20) for the symmetric case $N=Z$, we write

$$E_{\rm tot}(\rho_0,A,X=0)/A = e_0(\rho_0) + b_S(\rho_0)A^{-1/3} + \alpha_C(\rho_0)A^{2/3}, \tag{42}$$

where ρ_0 is related to the equimolar radius R_e as in Eq. (21). Assuming that $\tilde{\rho}_{0,\rm eq}$ is the equilibrium density for the

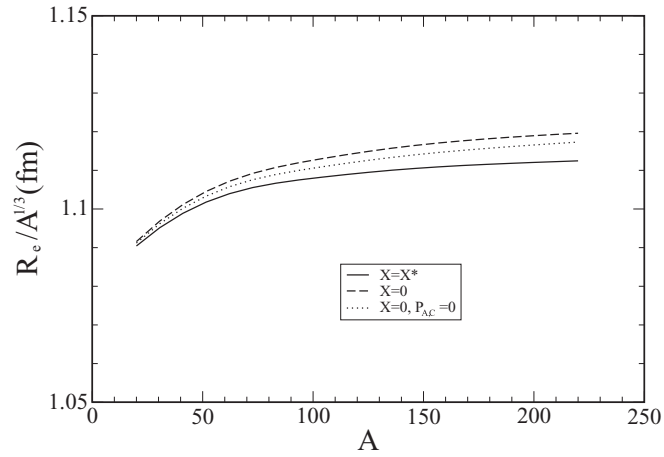

FIG. 3. Dependence of equimolar radius $R_e = R_e^*(A,X^*)$ on mass number A on the β-stability line in the presence of the polarization effect (the solid line). The dashed line is the equimolar radius $R_e(A,X=0)$ where the polarization effect is absent. The dotted line is obtained by elimination of the Coulomb force polarization effect, see Eq. (46). The calculations were performed for the SkM* [15] interaction.

uncharged liquid drop, we will expand the total energy of Eq. (42) around the equilibrium density $\tilde{\rho}_{0,\mathrm{eq}}$ as

$$\frac{E_{\mathrm{tot}}(\rho_0,A,X=0)}{A} = \frac{E_{\mathrm{tot}}(\tilde{\rho}_{0,\mathrm{eq}},X=0)}{A} + \frac{K_A(A,X=0)}{18\tilde{\rho}^2_{0,\mathrm{eq}}}(\rho_0-\tilde{\rho}_{0,\mathrm{eq}})^2 + \frac{P_{A,C}(\tilde{\rho}_{0,\mathrm{eq}})}{\tilde{\rho}^2_{0,\mathrm{eq}}}(\rho_0-\tilde{\rho}_{0,\mathrm{eq}}), \quad (43)$$

where

$$P_{A,C}(\rho_0) = \rho_0^2\frac{\partial}{\partial\rho_0}\alpha_C(\rho_0)A^{2/3} \quad (44)$$

is the Coulomb force pressure. The equilibrium density $\rho_{0,\mathrm{eq}}$ of a symmetric nucleus in the presence of Coulomb forces is obtained from the condition,

$$\frac{\partial}{\partial\rho_0}E_{\mathrm{tot}}(\rho_0,A,X=0)/A\Big|_{A,\rho_0=\rho_{0,\mathrm{eq}}} = 0. \quad (45)$$

Using Eqs. (37), (39), and (45), one obtains the polarization effect on the particle density caused by Coulomb forces for symmetric nuclei with $N=Z$,

$$\rho_{0,\mathrm{eq}} = \tilde{\rho}_{0,\mathrm{eq}} - 9\frac{P_{A,C}(\tilde{\rho}_{0,\mathrm{eq}})}{K_A(A,X=0)}. \quad (46)$$

The Coulomb force pressure is positive $P_{A,C}(\rho_0)>0$, see Eqs. (22) and (44), and thereby the polarization effect, which is caused by the Coulomb forces, decreases the bulk density $\rho_{0,\mathrm{eq}}$, i.e., increases the nuclear equimolar radius R_e of Eq. (21). The corresponding numerical result is shown in Fig. 3 as the dotted line.

IV. NUCLEAR RADII

Using the experimental values [22] of the chemical potentials λ and λ_- for the arbitrary dividing radius R and the fixed asymmetry parameter X, one can evaluate the volume part of equilibrium energy $E_{\mathcal{V}}$ from Eq. (10), and the particle numbers in the volume $A_{\mathcal{V}}=4\pi\rho R^3/3$ and $A_{-,\mathcal{V}}=4\pi\rho_- R^3/3$ and in the surface $A_{\mathcal{S}}=4\pi\rho_{\mathcal{S}}R^2$ and $A_{-,\mathcal{S}}=4\pi\rho_{-,\mathcal{S}}R^2$ particle numbers. All these evaluated values depend on the radius R of the dividing surface and the asymmetry parameter X.

As noted above, the actual physical radius R_e of the nucleus is determined by the condition (14), i.e., by the requirements that the contribution to $E_{\mathcal{S}}$ from the bulk binding energy [term $\sim(\rho_{\mathcal{S}}\lambda+\rho_{-,\mathcal{S}}\lambda_-)$ in Eq. (3)] should be excluded from the surface energy $E_{\mathcal{S}}$. In Fig. 4 we represent the results of the calculation of the specific surface particle density $F(R)=-(\rho_{\mathcal{S}}\lambda+\rho_{-,\mathcal{S}}\lambda_-)$ as a function of radius R of the dividing surface. The equimolar dividing radius R_e in Fig. 4 defines the physical size of the sharp surface droplet and the surface at which the surface tension is applied, i.e., the equimolar surface where Eq. (14) is fulfilled.

The evaluated equimolar radius R_e does not necessarily obey the saturation condition $R_e\sim A^{1/3}$. This reflects the fact that the experimental data for the chemical potentials λ and λ_- used in our calculations include the quantum shell effects, the pairing correlation effects, etc. In Fig. 5 we have plotted

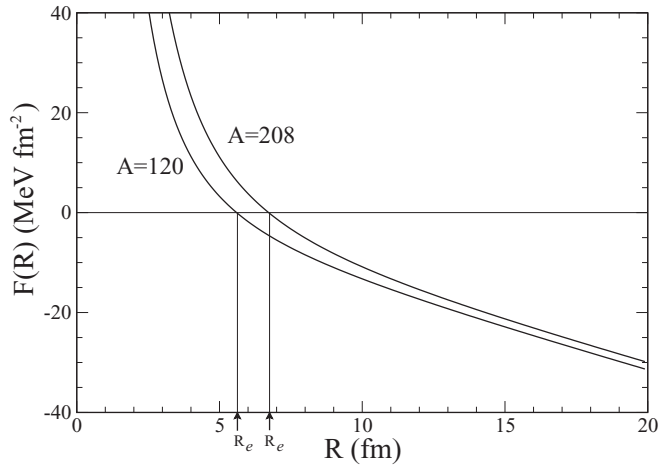

FIG. 4. Specific surface particle density $F(R)=-(\rho_{\mathcal{S}}\mu+\rho_{-,\mathcal{S}}\mu_-)$ versus dividing radius R for nuclei with $A=208$ and $A=120$. The calculation was performed using the SkM* interaction [15]. R_e denotes the equimolar radius where $F(R)=0$.

the evaluated equimolar radii R_e for some nuclei. The dotted line shows the average behavior $R_e=r_0A^{1/3}$.

We point out that the average interparticle distance r_0 is slightly A dependent (see the dashed line in Fig. 5),

$$r_0\approx\left(1.14-\frac{0.04}{A^{1/3}}\right)\ \mathrm{fm}. \quad (47)$$

The nonmonotonic behavior of the nuclear equimolar radii $R_e(A)$ is caused by the quantum shell fluctuations, the pairing effects, etc., which are manifested in the experimental values of the chemical potentials λ_n and λ_p.

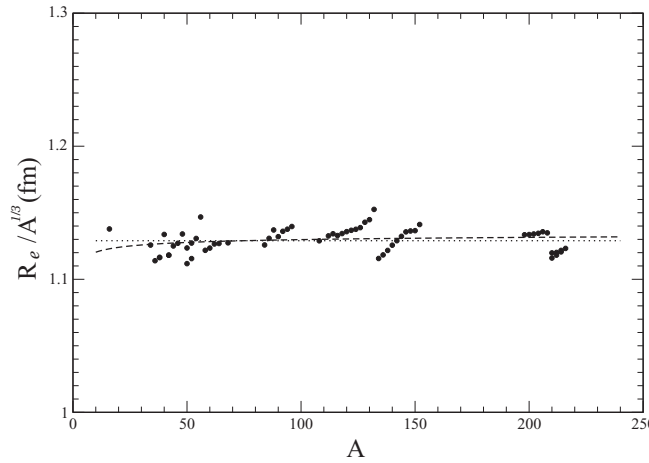

FIG. 5. A dependence of equimolar nuclear radius $R_e(A)$. The solid points were obtained within the Gibbs-Tolman procedure where the experimental values for the nucleon chemical potential were used, and the dashed line is for the corresponding averaged values of equimolar radii R_e. The dotted line is for $R_e=1.13A^{1/3}$ fm. The SkM* interaction [15] was used.

V. SKIN AND HALO EFFECTS—ISOVECTOR SHIFT OF THE RADII

The above-described procedure can be used to derive the partial equimolar radii $R_{e,q}(A)$ separately for neutrons $q = n$ and for protons $q = p$ and the corresponding nucleon rms radii $\sqrt{\langle r_q^2\rangle}$. Using the experimental values of the chemical potentials λ_n and λ_p of actual nuclei and Eqs. (10)–(13), one can derive the partial bulk densities ρ_n and ρ_p. Evaluating then the partial surface nucleon densities,

$$\rho_{n,S}[R] = \frac{N}{4\pi R^2} - \frac{1}{3}\rho_n R, \quad \rho_{p,S}[R] = \frac{Z}{4\pi R^2} - \frac{1}{3}\rho_p R, \tag{48}$$

and applying the condition of Eq. (14), we find the partial equimolar radii $R_{e,q}(A)$. Considering the rms radii,

$$\sqrt{\langle r_q^2\rangle} = \sqrt{\int d\boldsymbol{r}\; r^2\rho_q(r) \Big/ \int d\boldsymbol{r}\; \rho_q(r)}, \tag{49}$$

in the presence of the finite diffuse layer, we will introduce the dispersion of the surface layer [1],

$$b_q = \sqrt{\int_o^\infty dr\; g_q(r)(r-\bar{r}_q)^2}, \tag{50}$$

where

$$g_q(r) = -d\frac{f_q(r)}{dr}, \; \bar{r}_q = \int_0^\infty dr\; r g_q(r),$$

and $f_q(r) = \rho_q(r)/\rho_{0,q}$ is the profile function of the nucleon density.

In the case of the Fermi-like profile function $f(r)$ of Eq. (18), one obtains

$$b_q = a_q\sqrt{[2\kappa_1(\eta_q) - \kappa_0^2(\eta_q)]}, \tag{51}$$

where the coefficients $\kappa_i(\eta)$ are given by [6]

$$\kappa_i(\eta) = \int_0^\infty dx\; x^i\{(1+e^x)^{-\eta} - (-1)^i[1-(1+e^{-x})^{-\eta}]\}. \tag{52}$$

Finally, the nucleon rms radii read, see also Ref. [1],

$$\sqrt{\langle r_q^2\rangle} \approx \sqrt{3/5}R_{e,q}\left[1 + \frac{5}{2}\left(\frac{b_q}{R_{e,q}}\right)^2\right]. \tag{53}$$

Note that the surface layer correction $\sim b_q^2$ to the rms radii in Eq. (53) can exceed the value of about 10% in light and middle nuclei. We also point out that the rms radii $\sqrt{\langle r_q^2\rangle}$ of Eq. (53) as well as the equimolar radii $R_{e,q}(A)$ contain the shell fluctuations, see Fig. 5.

The partial equimolar radius $R_{e,q}$ and the corresponding rms radii $\sqrt{\langle r_q^2\rangle}$ can be evaluated numerically from Eqs. (10)–(13) and (53) using the chemical potentials λ_n and λ_p of actual nuclei. As an example we will show the result for the ^{208}Pb nucleus. In this case, using the variational procedure of Eq. (19) and trial function for $\rho_q(\boldsymbol{r})$ of Eq. (18), we obtain for the SkM* interaction $a_n = 0.723, a_p = 0.618$ fm, $\eta_n = 4.048$, and $\eta_p = 5.158$. Using the average interparticle distance r_0 from Eqs. (47) and (53), one obtains for the mass rms radius $\sqrt{\langle r^2\rangle} = 5.447$ fm, which agrees with experimental data $\sqrt{\langle r^2\rangle}|_{\rm exp} = (5.579 \pm 0.025)$ fm [27]. In Fig. 6, we also show the evaluated values of the proton rms radius $\sqrt{\langle r_p^2\rangle}$ for the Na isotopes. As seen from Fig. 6, the surface layer correction $\sim b_q^2$ in Eq. (53) leads to the significant shift up of $\sqrt{\langle r_p^2\rangle}$ with respect to the sharp radius estimate $\sqrt{\langle r_q^2\rangle} = \sqrt{3/5}R_q$ (compare the dashed and dotted lines) and provides the satisfactory agreement with experimental data. A slightly nonmonotonic behavior of $\sqrt{\langle r_p^2\rangle}$ in Fig. 6 is caused by the above-mentioned shell fluctuations of $R_{e,p}$.

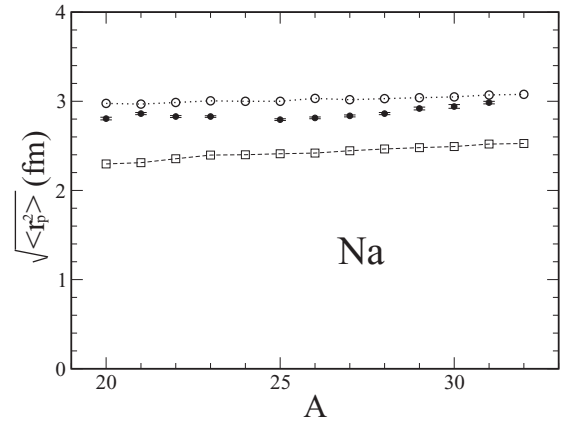

FIG. 6. The rms radius of the proton distribution in the Na isotopes obtained by use of Eq. (53). The dotted line with open circles was obtained with surface layer correction $\sim b_q^2$, and the dashed line with open squares is for $b_q^2 = 0$. Here and below, the experimintal data were taken from Ref. [24]. The SkM* interaction [15] was used.

Evaluating the isovector shift of particle density ρ_-, one can determine the neutron-skin thickness $\Delta r_{np} = \sqrt{\langle r_n^2\rangle} - \sqrt{\langle r_p^2\rangle}$.

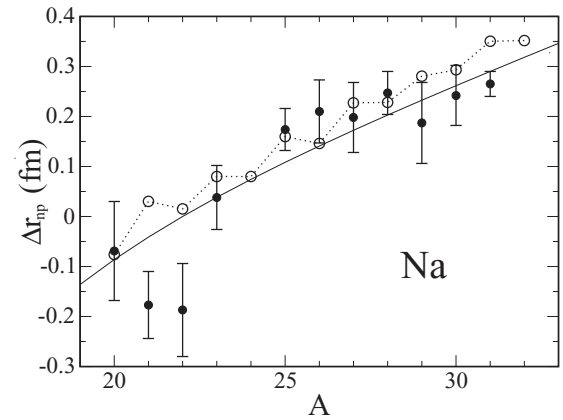

FIG. 7. The isovector shift of nuclear rms radius $\Delta r_{np} = \sqrt{\langle r_n^2\rangle} - \sqrt{\langle r_p^2\rangle}$ in Na isotopes. The solid points are the experimental data [24], the open circles (connected by the dotted line) have been obtained using the Gibbs-Tolman approach described in the text, and the solid line is obtained using the extended Thomas-Fermi approximation with the SkM* Skyrme interaction [15], see Ref. [6].

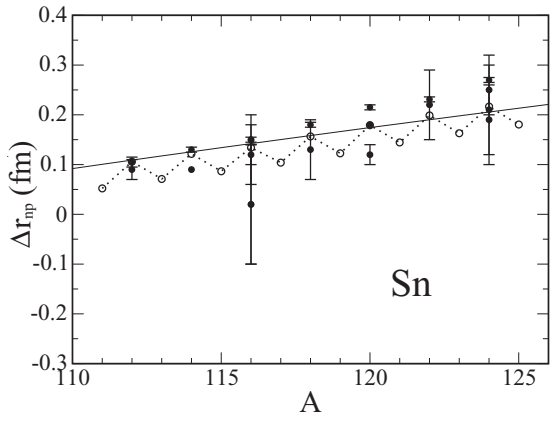

FIG. 8. The same as in Fig. 7 but for Sn isotopes. The data were taken from Refs. [23,25,26].

The A dependence of the size of the neutron-skin thickness Δr_{np} is illustrated in Figs. 7–9 for Na, Sn, and Pb isotopes, respectively. Here, the experimental data were taken from Refs. [23–29]; the results obtained using the Gibbs-Tolman-Rowlinson-Widom approach are shown by the open circles, and the solid line is obtained within the extended Thomas-Fermi approximation with Skyrme interactions [6].

As seen from Figs. 7–9, the Gibbs-Tolman-Rowlinson-Widom concept of the sharp equimolar surface allows one to describe the fine nonmonotonic structure of the nucleon rms radius and thereby the isovector shift Δr_{np}. In particular, the sawlike behavior of Δr_{np} (see the open circles which are connected by the dotted line) reflects the even-odd and shell effects in the nuclear binding energy and thereby in the nuclear radii.

In general, the value of the isovector shift Δr_{np} is the sum of two contributions: One $\Delta r_{np,R}$ is due to the different radii (skin effect), and the other $\Delta r_{np,a}$ is due to the different shapes (surface layer) of the neutron and proton distributions (halo

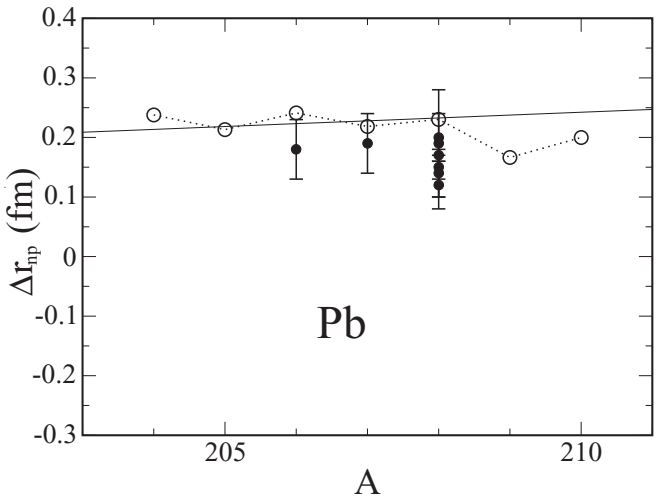

FIG. 9. The same as in Fig. 7 but for Pb isotopes. The experimental data were taken from Refs. [27–29].

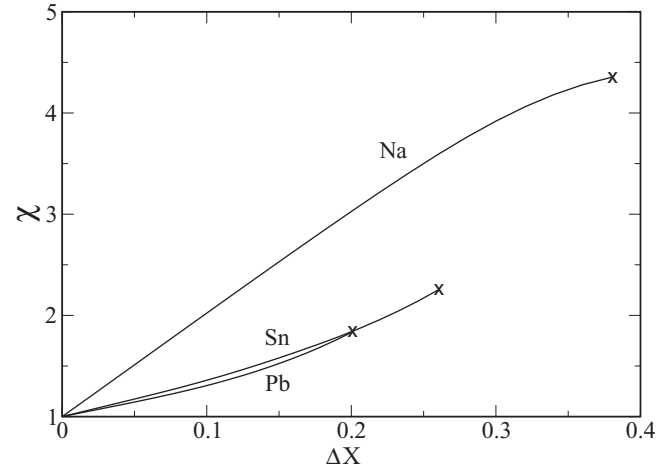

FIG. 10. The ratio $\chi = \Delta r_{np,a}/\Delta r^*_{np,a}$ versus the deviation $\Delta X = X - X^*$ from the β-stability line for isotopes of the nuclei of Na, Sn, and Pb. The calculations have been performed using the SkM* interaction [15] and Weizsecker's parameter $\beta = 1/9$ [see Eq. (15)]. The crosses at the end of the lines denote the neutron drip line, which is derived by the condition $\lambda_n = 0$.

effect), see also Refs. [25,26,30–32],

$$\Delta r_{np} = \Delta r_{np,R} + \Delta r_{np,a}, \tag{54}$$

Both values of $\Delta r_{np,R}$ and $\Delta r_{np,a}$ can be obtained from Eq. (53) and are given by the following expressions:

$$\Delta r_{np,R} \approx \sqrt{\frac{3}{5}}\left[1 - \frac{5}{2}\left(\frac{b}{R_e}\right)^2\right]\Delta_{R,e}, \tag{55}$$

and

$$\Delta r_{np,a} \approx 5\sqrt{\frac{3}{5}}\frac{b}{R_e}\Delta_b. \tag{56}$$

Here, $\Delta_{R,e} = R_{e,n} - R_{e,p}$, $b = (b_n + b_p)/2$, and $\Delta_b = b_n - b_p$ are the parameters of the neutron skin.

Expressions (54)–(56) dissect the structure of the neutron-skin thickness Δr_{np}. In Fig. 10 we have plotted the values of $\chi = \Delta r_{np,a}/\Delta r^*_{np,a}$ (the value of $\Delta r^*_{np,a}$ is taken on the β-stability line at $X = X^*$) versus the deviation $\Delta X = X - X^*$ from the β-stability line $X = X^*$ for the neutron-rich ($\Delta X > 0$) isotopes of the nuclei of Na, Sn, and Pb.

The numerical results for $\Delta r_{np,a}$ are sensitive to the choice of the gradient corrections to the kinetic-energy density $\epsilon_{\mathrm{kin},q}[\rho_q]$ [see the term with the parameter β in Eq. (15)]. In Fig. 10, we have used the empirical value for Weizsäcker's parameter $\beta = 1/9$. Note also that evaluating the skin parameter $\Delta_{R,e}$ in Eq. (55) we have used the Gibbs-Tolman-Rowlinson-Widom procedure, which is described in Sec. II. As can be seen from Fig. 10, the relative contribution of the shape (halo) effect, i.e., $\Delta r_{np,a}$, to the isotopic shift of radii Δr_{np} is more evident in the light nuclei. As can be expected, the ratio $\Delta r_{np,a}/\Delta r^*_{np,a}$ increases for nuclei away from the β-stability line, i.e., for the neutron-rich isotopes.

VI. CONCLUSIONS

We have applied the approach proposed earlier by Gibbs-Tolman-Rowlinson-Widom for a classical liquid drop in the presence of the liquid-vapor interface to the derivation of the actual size of a nucleus in the presence of a finite surface diffuse layer. The basic idea of the Gibbs-Tolman-Rowlinson-Widom approach is the introduction of a sharp dividing surface $\mathcal{S}$ [2–4]. The dividing surface is arbitrary but located within the surface diffuse layer. The actual (physical) equimolar surface and thereby the actual nuclear surface are fixed by the requirement that the contribution to the surface energy $E_S[R] \sim A^{2/3}$ from the bulk energy $E_{\rm bulk} \sim A$ should be eliminated, see Eq. (14). The bulk density ρ_0 of the neutrons and protons inside the sharp equimolar surface is obtained using the experimental data for the separation energy s_q for each kind of nucleon.

The Gibbs-Tolman-Rowlinson-Widom conception of a sharp equimolar surface allows one to derive the nuclear volume and, as a consequence, the pressure $P(\rho_0)$ and the equation of state for finite nuclei. In our consideration, we have performed the calculations of a well-defined equation of state for spherical nuclei and some nuclear characteristics, such as the nuclear radius, the surface tension, the pressure, etc. Our numerical calculations are based on the direct variational method, the extended Thomas-Fermi approximation, and the effective Skyrme nucleon-nucleon interaction. Applying the Gibbs-Tolman-Rowlinson-Widom approach, we redefine the surface and symmetry energies. Note that we do not use the traditional leptodermous approximation and evaluate the Coulomb energy taking into consideration the finite diffuse layer of the proton distribution.

Performing the analysis of the equation of state $P = P(\rho_0)$, we have extracted from $P(\rho_0)$ the partial contributions which occur due to the different sources: the A- and X-independent bulk pressure $P_{\rm vol}(\rho_0)$ caused by the bulk energy of a symmetric nuclear matter, the surface (capillary) pressure $P_{A,\rm capil}(\rho_0, X) \sim A^{-1/3}$, the contribution from the symmetry energy $P_{A,\rm sym}(\rho_0, X) \sim X^2$, and the Coulomb force contribution $P_{A,C}(\rho_0, X)$. The corresponding numerical results are shown in Fig. 1 for the ^{208}Pb nucleus. The inclusion of the surface (capillary) term $P_{\rm capil}(\rho_0, X)$ shifts the equilibrium point $\rho_{0,\rm eq}$ to larger values with respect to the ones in a nuclear matter. Note also that the capillary pressure $P_{A,\rm capil}(\rho_0, X)$ is connected to the surface tension coefficient $\sigma(A, X)$ by the classical Laplace relation. The action of the Coulomb pressure $P_{A,C}(\rho_0, X)$ is opposite the capillary pressure $P_{A,\rm capil}(\rho_0, X)$ and shifts the equilibrium point to the smaller values of $\rho_{0,\rm eq}$.

The use of the Gibbs-Tolman-Rowlinson-Widom equimolar radius R_e allowed us to give a more realistic procedure for an extraction of the nuclear surface tension coefficient from the experimental data. The equimolar radius R_e determines the equimolar surface area S_e in the absence of a diffuse layer. This fact allows us to evaluate both the surface energy E_{S_e} and the surface tension coefficient $(A, X) = E_{S_e}/S_e$. Using the experimental data within the wide interval of mass number $40 \leqslant A \leqslant 220$ and the corresponding values of equimolar radii, we have established the following A expansion for the surface tension coefficient $\sigma(A, X^*) = \sigma_0 + \sigma_1 A^{-1/3}$ with $\sigma_0 = (0.98 \pm 0.03)$ and $\sigma_1 = (0.75 \pm 0.16)$ MeV fm^{-2}. The obtained result for the curvature correction $\sigma_1 A^{-1/3}$ allows one to estimate the Tolman length ξ in nuclei, which is $\xi = (-0.41 \pm 0.07)$ fm.

We have evaluated the partial pressure $P_{A,\rm sym}(\rho_0, X)$ caused by the symmetry energy. The partial pressure $P_{A,\rm sym}(\rho_0, X)$ induces the polarization effect on the particle density $\rho_{0,X}$ beyond the β-stability line. We have shown that the partial pressure $P_{A,\rm sym}(\rho_{0,\rm eq})$ is positive and reduces the particle density $\rho_{0,X}$ with respect the corresponding equilibrium density $\rho_{0,\rm eq}$ on the β-stability line. The partial pressure $P_{A,\rm sym}$ and the polarization effect are rather sensitive to the Skyrme interaction parametrization (see the results for the SkM*, SLy230b, and KDE0v1 in Fig. 2). We point out that the evaluated equimolar radius R_e of the nuclei does not necessarily obey the saturation condition $R_e = r_0 A^{1/3}$. That is caused by the fact that we use the experimental data for the chemical potentials to derive the bulk density within the equimolar surface in agreement with the Gibbs-Tolman-Rowlinson-Widom method. The corresponding experimental chemical potentials (separation energy of nucleons) include the quantum shell effects, the pairing correlation effects, etc., and give rise to the nonmonotonic behavior of the nuclear equimolar radii $R_e(A)$ in Fig. 5. Note also that the average interparticle distance r_0 becomes slightly A dependent (see the dashed line in Fig. 5).

Using the partial equimolar radii $R_{e,q}(A)$ separately for both kinds of nucleon, we have evaluated the corresponding nucleon rms radii $\sqrt{\langle r_q^2\rangle}$ and the neutron-skin thickness $\Delta r_{np} = \sqrt{\langle r_n^2\rangle} - \sqrt{\langle r_p^2\rangle}$. The evaluated values of the proton rms radius $\sqrt{\langle r_p^2\rangle}$ for the Na isotopes (see Fig. 6) show a slightly nonmonotonic behavior of $\sqrt{\langle r_p^2\rangle}$, which is caused by the above-mentioned fluctuations of $R_{e,p}$. Note also the presence of the significant shift up of the proton rms $\sqrt{\langle r_p^2\rangle}$ (compare the dashed and dotted lines in Fig. 6) caused by the surface layer corrections. The influence of the pairing and shell effects on the neutron-skin thickness Δr_{np} is illustrated in Figs. 7–9 for Na, Sn, and Pb isotopes. As seen from Figs. 7–9, the Gibbs-Tolman-Rowlinson-Widom concept of the sharp equimolar surface allows one to describe a fine nonmonotonic structure of the isovector shift Δr_{np}. The sawlike behavior of Δr_{np} (see the open circles which are connected by the dotted lines in these figures) reflects the even-odd and shell effects in the nuclear binding energy and thereby in the nuclear radii. In general, the value of the isovector shift Δr_{np} is the sum of two contributions: One $\Delta r_{np,R}$ is due to the different radii (skin effect), and the other $\Delta r_{np,a}$ is due to the different shapes (surface layer) of the neutron and proton distributions (halo effect). The presence of the halo effect is illustrated in Fig. 10. One can expect that the neutron halo effect appears more significantly in light nuclei far away from the stability line.

ACKNOWLEDGMENTS

This work was supported, in part, by the National Academy of Sciences of Ukraine under Grant No. CO-2-14/2016 (V.M.K., S.V.L., and A.I.S.) and by the U.S. Department of Energy under Contract No. DOE-FG03-93ER40773 (S.S.). S.S. also thanks the Weizmann Institute for the Weston Visiting Professorship Award and the nice hospitality extended to him.

[1] W. D. Myers, Nucl. Phys. A **204**, 465 (1973).
[2] J. W. Gibbs, *Collected Works* (Longmans, Green, New York, 1928), Vol. I.
[3] R. C. Tolman, J. Chem. Phys. **17**, 333 (1949).
[4] J. S. Rowlinson and B. Widom, *Molecular Theory of Capillarity* (Clarendon, Oxford, 1982).
[5] V. M. Kolomietz and A. I. Sanzhur, Eur. Phys. J. A **38**, 345 (2008).
[6] V. M. Kolomietz, S. V. Lukyanov, and A. I. Sanzhur, Phys. Rev. C **85**, 034309 (2012).
[7] V. M. Kolomietz, S. V. Lukyanov, and A. I. Sanzhur, Phys. Rev. C **86**, 024304 (2012).
[8] L. D. Landau and E. M. Lifshitz, *Statistical Physics* (Pergamon, Oxford, 1958).
[9] V. M. Kolomietz and A. I. Sanzhur, Phys. Rev. C **88**, 044316 (2013).
[10] D. A. Kirzhnitz, *Field Theoretical Methods in Many Body Systems* (Pergamon, London, 1967).
[11] W. D. Myers and W. J. Swiatecki, Ann. Phys. (NY) **55**, 395 (1969).
[12] W. D. Myers and W. J. Swiatecki, Ann. Phys. (NY) **84**, 186 (1974).
[13] P. Möller, J. R. Nix, W. D. Myers, and W. J. Swiatecki, At. Data Nucl. Data Tables **59**, 185 (1995).
[14] P. Danielewicz, Nucl. Phys. A **727**, 233 (2003).
[15] M. Brack, C. Guet, and H.-B. Haakansson, Phys. Rep. **123**, 275 (1985).
[16] L. D. Landau and E. M. Lifshitz, *Fluid Mechanics* (Pergamon, London, 1959).
[17] M. J. P. Nijmeijer, C. Bruin, A. B. van Woerkom, and A. F. Bakker, J. Chem. Phys. **96**, 565 (1992).
[18] E. Chabanat, R Bonche, R Haensel, J. Meyer, and R. Schaeffer, Nucl. Phys. A **635**, 231 (1998).
[19] B. K. Agrawal, S. Shlomo, and V. K. Au, Phys. Rev. C **72**, 014310 (2005).
[20] K. Oyamatsu, I. Tanichata, S. Sugahara, K. Sumiyoshi, and H. Toki, Nucl. Phys. A **634**, 3 (1998).
[21] K. Oyamatsu and K. Iida, Prog. Theor. Phys. **109**, 631 (2003).
[22] G. Audi, A. H. Wapstra, and C. Thibault, Nucl. Phys. A **729**, 337 (2003).
[23] L. Ray, Phys. Rev. C **19**, 1855 (1979).
[24] T. Suzuki, H. Geissel, O. Bochkarev *et al.*, Phys. Rev. Lett. **75**, 3241 (1995).
[25] A. Trzcińska, J. Jastrzębsky, P. Lubiński, F. J. Hartmann, R. Schmidt, T. von Egidy, and B. Kłos, Phys. Rev. Lett. **87**, 082501 (2001).
[26] A. Krasznahorskay, H. Akimune, A. M. van den Berg *et al.*, Nucl. Phys. A **731**, 224 (2004).
[27] V. E. Starodubsky and N. M. Hintz, Phys. Rev. C **49**, 2118 (1994).
[28] S. Karataglidis, K. Amos, B. A. Brown, and P. K. Deb, Phys. Rev. C **65**, 044306 (2002).
[29] B. C. Clark, L. J. Kerr, and S. Hama, Phys. Rev. C **67**, 054605 (2003).
[30] S. Mizutori, J. Dobaczewski, G. A. Lalazissis, W. Nazarewicz, and P.-G. Reinhard, Phys. Rev. C **61**, 044326 (2000).
[31] M. Warda, X. Viñas, X. Roca-Maza, and M. Centelles, Phys. Rev. C **81**, 054309 (2010).
[32] M. Centelles, X. Roca-Maza, X. Viñas, and M. Warda, Phys. Rev. C **82**, 054314 (2010).